Attenuation performance of geosynthetic sorption sheets against arsenic subjected to compressive stresses

AUTHOR(S):

Zhang, Yu; Kinoshita, Yosuke; Kato, Tomohiro; Takai, Atsushi; Katsumi, Takeshi

CITATION:

Zhang, Yu ...[et al]. Attenuation performance of geosynthetic sorption sheets against arsenic subjected to compressive stresses. Geotextiles and Geomembranes 2023, 51(5): 179-190

ISSUE DATE:

2023-10

URL:

http://hdl.handle.net/2433/284449

Geotextiles and Geomembranes 51 (2023) 179–190

Contents lists available at ScienceDirect

Geotextiles and Geomembranes

journal homepage: www.elsevier.com/locate/geotexmem

Regular Paper

Attenuation performance of geosynthetic sorption sheets against arsenic subjected to compressive stresses

Yu Zhang [a,*], Yosuke Kinoshita [b], Tomohiro Kato [a], Atsushi Takai [a], Takeshi Katsumi [a]

[a] Graduate School of Global Environmental Studies, Kyoto University, Kyoto, 606-8501, Japan
[b] Graduate School of Engineering, Kyoto University, Kyoto, 606-8501, Japan

ARTICLE INFO

Keywords:
Attenuation layer method
Arsenic
Geosynthetics
Hydrotalcite
Sorption
Compressive stress

ABSTRACT

The attenuation layer method has been considered an effective countermeasure to deal with excavated soils and rocks containing geogenic toxic elements like arsenic (As). The geosynthetic sorption sheet is a geosynthetic product that can be employed in the attenuation layer method applications as a sorption material. The sorption sheets used in the attenuation layer will be inevitably subjected to overburdened loads in the field. In this study, laboratory column experiments are conducted to evaluate the attenuation performance of the geosynthetic sorption sheets coated with hydrotalcite as sorbent against As under different overburden pressure conditions (10, 100, and 200 kPa). Experimental results showed that the cumulative sorption masses of As for 200 kPa cases are approximately 10.5–13.3 times greater than that for 10 kPa cases. Microstructure characterizations of the geosynthetic sorption sheet before and after loading were also detected. More compacted and involved fiber configuration as a result of higher loading produces a more effective contact between As solution and hydrotalcite. The presence of partial dissolution of hydrotalcite is confirmed through the chemical analysis of effluent. However, hydrotalcite would gradually become stable during continuous use.

1. Introduction

Large volumes of excavated soils and rocks (ESR) is generated as a by-product of the various construction works (Katsumi, 2015; Osono and Katoh, 2021). The Japanese Ministry of Land, Infrastructure, Transport, and Tourism (MLIT, 2018) reported that in the past few decades, more than 280 million m^3 of ESR were annually produced in Japan. Numerous studies have indicated that rapid expansion and improper management of excavation materials spark growing adverse impacts on the environment, economy, and society (Duan et al., 2015, 2019; Wang et al., 2004; Zhang et al., 2020). In responding to such problems, how properly managing the surplus ESR becomes to be an important issue in many countries (Qian et al., 2019). Some studies have confirmed the feasibility of ESR as construction material, and reported that it is the preferred material for embankment constructions in road- and railway-tunnel projects (Riviera et al., 2014; Lieb, 2009; Tabelin et al., 2017, 2018). In spite of the utilization of excavated materials are the future development pattern of construction works, environmental consequences brought by its use are an indispensable component in practical procedures (Haas et al., 2021; Duan et al., 2015; Magnusson et al., 2015).

Arsenic (As) contamination, as a universal problem of geological origin, exists in geologic strata around the world (Buccino et al., 2021; Somma et al., 2021). In general, these soil/rock materials from deep excavations are rarely subjected to anthropogenic disturbance and often contain As contents at levels closer to the background level (Tabelin et al., 2012a; Katsumi, 2015; Jha and Tripathi, 2021). Therefore, such soils/rocks are usually recognized by default as non-hazardous in sustainable project management (Li et al., 2017; Tabelin et al., 2014a, 2017, 2018). However, it has been found that variations in the external environment of ESR caused by construction works and excavation activities, such as increased specific surface area, exposure to oxygen and water, and drying, enhance the risk of As being released into the surrounding environment (Tabelin et al., 2013, 2014b; Osono and Katoh, 2021; Li et al., 2018; Tangviroon et al., 2017; Cui et al., 2018). The leaching concentration of As from ESR typically tends to slightly exceed the Japanese environmental standard (10 μg/L) (Osono and Katoh, 2021; Kato et al., 2023). This situation effectively indicates that ESR containing As may negatively impact the surrounding environment if it is applied to construction projects or directly stacked in the temporary

* Corresponding author.
E-mail address: zhang.yu.a44@kyoto-u.jp (Y. Zhang).

https://doi.org/10.1016/j.geotexmem.2023.06.004
Received 28 September 2022; Received in revised form 8 June 2023; Accepted 18 June 2023
Available online 30 June 2023

storage areas for future use without appropriate countermeasures. Therefore, cost-effective countermeasures should be explored for effectively and sustainably managing these naturally contaminated soils/-rocks from deep excavation.

The attenuation layer method, a low contamination-oriented countermeasure, has been newly developed in recent years for managing large quantities of ESR (Mo et al., 2020). Structurally, it can be simply described as installing a permeable attenuation layer with sorption capacity at the bottom of contaminated soils/rocks (Technical Committee of Environmental Conservation Technology Association). In this technique, water is allowed to penetrate into the waste, and the consequent leachate would then flow through the attenuation layer, during which hazardous elements are immobilized (Tatsuhara et al., 2012). Descending the concentration of hazardous elements effectively to the limited value before reaching groundwater aquifers is believed to be a crux of the attenuation layer method. It follows that the selection and utilization of low-cost and efficient materials are the main development tendency of the attenuation layer method.

A geosynthetic sheet with sorption capacity has recently been developed as a promising material for the attenuation layer method. The geosynthetic sorption sheet is presented in a sheet-shaped format, assembled by a non-woven fabric layer and a sorption material layer. This geosynthetic product can be used for different field applications as an attenuation sorption layer in either embankment constructions or temporary storage facilities, depending on the management practices of ESR (Magnusson et al., 2015). In these field practices, the geosynthetic sorption sheet is installed such that the non-woven fabric layer comes into contact with ESR, while the sorption material layer is in contact with the original ground. The function of the non-woven fabric layer is to control leachate transport effectively in the vertical as well as horizontal directions and thereby provide good contact between the contaminant and the underlying sorption material layer (Ding et al., 2021a). Besides, the mechanical support of this non-woven geotextile layer is essential to prevent the geosynthetic sorption sheet from being damaged during its service period (Ding et al., 2021b). The attenuation function is essentially implemented by the sorption material layer. The integration of these two functions helps to realize the expected end-use performance (attenuation performance) of geosynthetic sorption sheets.

In previous studies, this geosynthetic sorption sheet shows a high sorption capacity against hazardous elements like As (Inatomi et al., 2019; Shimoda et al., 2019). However, few studies have focused on the attenuation performance of sorption materials subjected to loading stress. The overburden load acting on the geosynthetic product is a factor that has to be considered in practical engineering. For example, for the temporary storage site, during its service, due to the continuous stacking and reuse of ESR, the thickness of which shows dynamic changes. This means the loading stress on the geosynthetic sorption sheets is inevitably different. Therefore, the influence of overburdened load on attenuation performance of geosynthetic sorption sheets needs to be evaluated to guarantee safe operation in practical projects.

The novelty of this study is that, for the first time, it investigates the effectiveness of the attenuation layer made of geosynthetic sorption sheets under different compressive stresses. To achieve this goal, the function reform of traditional consolidation instruments is firstly carried out to realize the operation of the sorption/desorption experiments under mechanical loadings. Then, a series of laboratory experiments are conducted to study the influence of compressive stress on the attenuation performance of geosynthetic sorption sheets against As. After that, the microstructures of the geosynthetic sorption sheet before and after loading are discussed to reveal the correlation between vertical loading and sorption performance. Moreover, the sorption discrepancy between As(III) and As(V) onto the geosynthetic sorption sheet is investigated. Finally, the chemical stability of the adsorbent contained in this studied geosynthetic material in aqueous solutions was evaluated.

2. Material and methods

2.1. Materials

The geosynthetic sorption sheet material (Fig. 1) used was provided by Toyobo Co., Ltd., Tokyo, Japan. The geosynthetic sorption sheet shows a closely-linked two-layer structure, with a thin and compacted sorption material layer containing hydrotalcite (hereafter referred to as hydrotalcite layer) and a non-woven fabric layer with long polyester fiber (hereafter referred to as fabric layer). Polyester fiber, as a typical hydrophobic fiber, tends to dispel water and prevent water from passing through (Cutright et al., 2020; Lin et al., 2022). Thus, a method for coating the surface of the fabric layer with hydrophilic materials was developed to facilitate hydrophilic functionalization, achieving stable sorption of solution containing contaminants. Hydrotalcites, the main class of layered double hydroxides compounds (LDH), are represented by $[Mg^{2+}_{(1-x)}\ Al^{3+}_{(x)}\ (OH)_2]^{x+}\ (A^{m-})_{x/m}{\cdot}mH_2O$ (Zubair et al., 2017). The term “hydrotalcite (HT)" is commonly used to refer to the LDH form in which the replaceable interlayer anion (A^{m-}) is CO_3^{2-} (Gillman, 2006). The hydrotalcite contained in the geosynthetic sorption sheet used in this study is chloride hydrotalcite with an Al/Mg molar ratio of 1:5–1:2. When the interlayer spacing is intercalated with other anions, such “hydrotalcite-type compounds” are differentiated in the literature by an anion prefix (e.g., NO_3-HT and PO_4-HT for nitrate and phosphate hydrotalcite, respectively) (Gillman, 2006; Dias and Fontes, 2020). In this study, the term “Cl-HT” was used to describe a particular LDH form consisting of Mg, Al, and Cl.

The basic physical properties of the geosynthetic sorption sheet provided by the manufacturer are shown in Table 1. The nominal thickness, hydraulic conductivity, and mass per unit area of the sorption sheet are found to be 2.8 mm, 1×10^{-3} m/s, and 450 g/m^2, respectively. Furthermore, the chemical composition analysis showed that this geosynthetic material is mainly composed of Mg, Al, and Cl (in a total of 85.4%), as well as a small quantity of Ti, S, Na, and Ca (in a total of 13.7%). The latter four components can be attributed to additives in processing.

As(V) and As(III) solutions were prepared by dissolving sodium dihydrogen arsenate (Na_2HAsO_4) and sodium arsenite ($NaAsO_2$) (Nacalai Tesque Inc., Kyoto, Japan) in distilled water, respectively.

2.2. Batch sorption experiments

All batch tests were carried out in 250-mL capped plastic bottles at room temperature (20 ± 2 °C) for a predetermined contact time. The mass of the sorbent was 0.2 g and mixed with 200 mL of solution in a liquid-to-solid ratio (L/S ratio) of 1000. A horizontal moving oscillation method was performed in all these experiments by a reciprocal oscillator (TS-10, TAITEC Co., Ltd.) running at 150 rpm, at an amplitude of 45 mm. All experiments were conducted in triplicate.

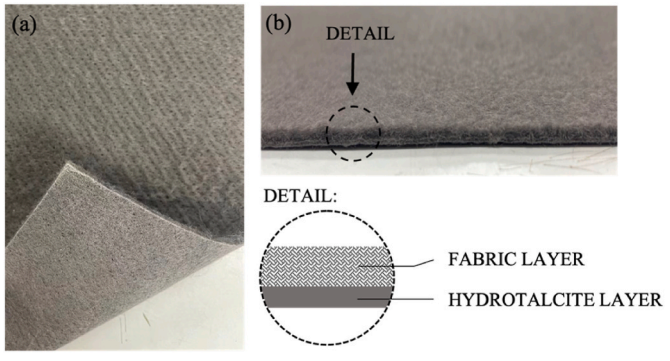

Fig. 1. The appearance of the geosynthetic sorption sheet. (a) Appearance; (b) Cross-section.

Table 1
Physical properties of geosynthetic sorption sheet.

Parameters	Values
Nominal thickness of the geosynthetic sorption sheet (mm)	2.8
Hydraulic conductivity (without compressive stress) (m/s)	1×10^{-3}
Mass per unit area of the geosynthetic sorption sheet (g/m^2)	450
Mass per unit area of the non-woven fabric (g/m^2)	310
Mass per unit area of Cl-HT (g/m^2)	50
Mass per unit area of other additives (g/m^2)	90

The equilibrium time of arsenic (As(III) and As(V)) sorption on the geosynthetic sorption sheet was first investigated by adjusting the contact time (ranging between 5 min and 24 h), and the initial concentration of As(III) and As(V) solution was fixed at 0.1 mg/L. To maintain a consistent sorbent mass of 0.2 g (see Table 1 for the mass per unit area of Cl-HT, which is 50 g/m^2), the geosynthetic sorption sheet was cut into pieces measuring 5 × 8 cm, which were then added to 200 mL of As solution with known concentrations. After the horizontal oscillation for the predetermined duration, the solid-liquid separation of samples was completed using a 0.45 μm-opening membrane filter, and the As concentration in the filtrate was evaluated.

The sorption equilibrium experiments were then conducted by varying initial concentrations of As(III) and As(V) (0.1, 1, 5, 10, 20 mg/L). The contact time of 24 h was set for achieving complete equilibrium by referring to sorption equilibrium time studies previously outlined. After 24 h of horizontal oscillation, solution samples were filtrated by 0.45 μm-opening membrane filters and then accessed for the analysis of As concentration.

The arsenic (As(III) and As(V)) sorption mass (S, mg/g) onto the geosynthetic sorption sheet at any time and arsenic (As(III) and As(V)) removal percentage (R, %), were determined from Eqs. (1) and (2), respectively (Liu et al., 2020; Lima et al., 2021):

$$S = \frac{(C_0 - C)V}{m} \tag{1}$$

$$R = \frac{C_0 - C}{C_0} \times 100 \tag{2}$$

where C_0 (mg/L) is the initial As concentration, C (mg/L) means the concentration of As at any time or equilibrium, V (mL) represents the volume of As solution, and m (g) refers to the mass of the adsorbent.

2.3. Column sorption-desorption experiments

2.3.1. Test apparatus

A novel column experimental setup, transformed from the traditional consolidation instrument (MIS-232-1-35, MARUI & Co., Ltd.), can simultaneously perform mechanical loading and percolation on geosynthetic materials to evaluate the As removal effect and estimate the loading-sorption relationship. A photograph and schematic diagram of the column test apparatus used in this study are presented in Fig. 2. It comprises a detachable permeameter device, a lever arm loading mechanism, a water-supply system, and an effluent reservoir. A low-carbon steel cylindrical column chamber of 2.0 cm height and 6.0 cm internal diameter, an acrylic top-loading cap of diameter 6.0 cm and a base plate constitute the detachable permeameter device. The column chamber was packed with the tailored sorption sheet specimen sandwiched with two porous stones.

The column chamber was set on the steel base. These two parts were accurately unified together with the aid of a specially designed 2.5 mm deep annular groove on the surface of the base plate, which is used to position and anchor the column chamber. A rubber gasket seal is adopted at the junction region to prevent bottom leakage effectively. A hole with a diameter of 4.0 mm is perforated in the center of the base and internally connected to a water inlet valve. The acrylic loading cap is placed on the top of the top porous stone, equipping holes for an outlet for effluent collection and a vent valve. A constant load applied by the lever arm mechanism acted directly on the acrylic loading cap, which was uniformly distributed on the geosynthetic sorption sheet.

2.3.2. Experimental procedure

The assembly of the equipment apparatus started from the column chamber. The cylindrical column chamber was placed onto the groove of the stainless steel base. Then, the sample combination was arranged into the column chamber in the order of porous stone, sorption sheet specimen, and porous stone. The sorption sheet specimen was uniformly spread by proper smooth to avoid fold defects. Porous stones were used to distribute the upward flow uniformly. The entire column permeameter setup was submerged in distilled water and saturated by a vacuum saturator (ASONE) for at least 24 h prior to being moved underneath the lever arm loading mechanism. After thorough saturation, the column chamber was subjected to continuous injection of arsenic (As(III) and As(V)) solution through the inlet valve of the base plate. A peristaltic pump (Thermo Fisher Scientific) was used to ensure a stable upward flow rate of 13–16 mL/h. Generally, the infiltration of precipitation into the embankment is about 30% (Ministry of the Environment), and, therefore, the flow rate in column tests is equivalent to the rainfall of 17 mm/h. The initial concentration for the arsenic (As(III) and As(V)) solution used in the column test was 0.1 mg/L.

The loading was applied on the geosynthetic sorption specimen via the lever arm mechanism to simulate the loading stress of a certain height of excavated soils/rocks in temporary storage sites or embankments. In this investigation, the vertical loads were taken at 10, 100, and 200 kPa, assuming three simplified field conditions employing a soils/rocks layer with a thickness of 0, 5, and 10 m over the sheet material, respectively. The effluent samples were collected periodically to measure the concentrations in the effluent. The sorption phase terminated when the effluent arsenic (As(III) and As(V)) concentration (C) approached the initial concentration (C_0), $C/C_0 = 0.95$.

The desorption test using As(V) solution was assessed immediately following the sorption phase. During the desorption phase, distilled water was applied to percolate through the column at the same flow rate until the As(V) concentration in effluent approximated 0.01 mg/L (Japanese environmental standard of arsenic). The sampling and subsequent measurements on samples were the same as the above sorption phase.

The column sorption and desorption test for porous stones alone were additionally carried out to eliminate a potential interference

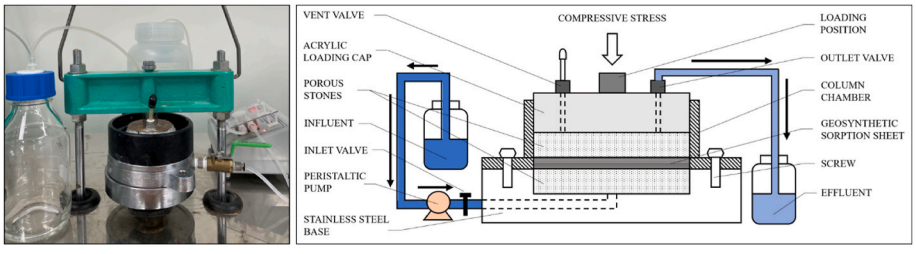

Fig. 2. Photograph and schematic diagram of the column test apparatus.

caused by the possible As(V) sorption capacity of porous stones. A load of 100 kPa was applied to the permeameter system during the column test for only porous stones. The experimental conditions of column tests are designed as presented in Table 2. All the experiments were performed at a constant room temperature of 20 ± 2 °C. After the experiments, the sorption sheet samples were then preserved by desiccation to evaluate the microstructure and other physicochemical qualities of the treated geosynthetics.

The cumulative sorption mass (S_s, mg/g) and desorption mass (S_d, mg/g) were determined using Eq. (3) and Eq. (4), respectively, as follows:

$$S_s = \sum_{s=1}^{n} \frac{(C_0 - C_s)V_s}{m} \tag{3}$$

$$S_d = \sum_{d=1}^{n} \frac{C_d V_d}{m} \tag{4}$$

where C_0 (mg/L) represents the influent concentration. C_s and C_d (mg/L) are effluent concentrations during the sorption and desorption process, respectively. V_s and V_d (L) are the volumes of permeated solution during the sorption and desorption process, respectively. M (g) is the mass of the adsorbent.

The immobility of As(V) on the geosynthetic sorption sheet can be evaluated by the immobilized fraction (Kato et al., 2021) and desorption ratio (D, %) (Junior et al., 2022). The immobilized fraction ($S_s - S_d$, mg/g) was specified as the difference between the cumulative sorption mass (S_s, mg/g) and desorption mass (S_d, mg/g), while D was evaluated by the ratio between S_s and S_d (Eq. (5)):

$$D = \frac{S_d}{S_s} \times 100 \tag{5}$$

2.4. Chemical and characterization analysis

The As concentration was analyzed by flame atomic adsorption spectrometry (AAS) (AA-6800, SHIMADZU). The concentration of other major elements in the effluent was measured using inductively coupled plasma optical emission spectrometry (ICP-OES) (710 ICP-OES, Agilent Technologies). The pH of effluent samples was analyzed by using a pH meter (F–54S, HORIBA). The morphological variations in geosynthetic sorption sheets before and after applied vertical loading were investigated using a scanning electron microscope (SEM) (JSM-6390LVS, JEOL). The chemical compositions of the geosynthetic samples were obtained by X-ray fluorescence (XRF) (EDX-720, SHIMADZU).

3. Results and discussion

3.1. Batch sorption experiments

3.1.1. Determination of sorption equilibrium time

Different reaction time intervals (5 min–24 h) were considered for investigating the optimal contact time to achieve sorption equilibrium of arsenic (As(III) and As(V)) on geosynthetic sorption sheets, at a fixed initial concentration of 0.1 mg/L. The experimental result of As sorption mass and removal percentage as a function of the contact time is presented in Fig. 3. It was observed that As sorption onto the geosynthetic sorption sheet exhibited a significant time-dependent manner. As displayed in Fig. 3, rapid sorption of both As(III) and As(V) was obtained during the first 1 h, and then sorption efficiency became slower, reaching an equilibrium condition gradually after 24-hrs of contact. The results indicated that at the initial concentration of 0.1 mg/L, the sorption mass of As(III) and As(V) was 0.093 and 0.097 mg/g, respectively, and their removal percentage was 93% and 97%, respectively, after the equilibrium time of 24 h. In general, the geosynthetic sorption sheet showed high efficiency in As sorption. Also worth noting that for As(V), more than 95% removal was achieved after the initial 15 min of contact. Afterward, the increasing extent of sorption mass gradually decreased until sorption equilibrium. The high sorption efficiency at the beginning of the sorption process depends mainly on the availability of reacting sites for the As(V) sorption on the geosynthetic sorption sheet (El-Sayed, 2011; Maamoun et al., 2021; Moosavi et al., 2020). Comparatively, as shown in Fig. 3, the removal percentage of As(V) was more than twice as much as that of As(III) at the initial stages. For instance, within the first 5 min of contact, the removal percentage was 37% and 85% for As(III) and As(V), respectively. Such results indicated that As(V) is sorbed by geosynthetic sorption sheets faster than As(III). For the subsequent sorption equilibrium study, the reaction time selected to reach equilibrium was 24 h.

Moreover, the monitored results of pH variation in the solution during the batch sorption process are presented in Fig. 4. The results indicate a consistent trend for both As(III) and As(V) cases. Specifically, the pH value increased rapidly with contact time during the early stage (5 min–4 h), from approximately 7.0–8.3, before plateauing and fluctuating around 8.4 after 24 h equilibrium time. The rise in pH during sorption is mainly involved with the sorbent, hydrotalcite, contained in the geosynthetic sorption sheet. Previous research reported a similar trend, revealing the partial dissolution of the hydrotalcite (Jobbágy and Regazzoni, 2011; Wei et al., 2011) (see the explanation in Section 3.3).

3.1.2. Sorption equilibrium study

The sorption mass and removal percentage at equilibrium with different initial As concentrations are illustrated in Fig. 5. Results depicted that the As sorption mass gradually increased with increasing initial concentration. The sorption mass of As(V) was always greater than that of As(III) at the same initial concentration, and in all cases, more than 97% of As(V) was removed from the aqueous solution. Whereas, for As(III), the removal percentage tended to decrease with the increase in its initial concentration, from 93% at low concentration (0.1 mg/L) to 67% at higher concentration (20 mg/L). These results show that geosynthetic sorption sheets have better performance of As(V) sorption in comparison to As(III) sorption. Consistent with several previous studies (e.g. Basu et al., 2014; Dias and Fontes, 2020; Sahu et al., 2011; Luo et al., 2018), arsenic could be removed or stabilized efficiently in its pentavalent form (As(V)). The reasons contributing to this phenomenon are analyzed further in the next section.

Nevertheless, it is undeniable that the geosynthetic sorption sheet is still efficient in As(III) sorption at a high concentration of up to 20 mg/L, with approximately 13.4 mg/g of As(III) sorbed onto it. In addition, the geosynthetic material showed no significant difference in the sorption for As(III) and As(V) at a low concentration of 0.1 mg/L, both the removal percentage reached to be above 90%.

Table 2
Experimental conditions of column tests.

Experimental phase	Solution	C_0 (mg/L)	Compressive stress (kPa)	Flow rate (mL/h)
Geosynthetic sorption sheet				
Sorption	As(III)	0.1	10, 200	13–16
Sorption	As(V)	0.1	10, 100, 200	13–16
Desorption	Distilled water	–		
Porous stone				
Sorption	As(V)	0.1	100	13–16
Desorption	Distilled water	–		

3.2. Column sorption-desorption experiments

3.2.1. Sorption phase

Figs. 6 and 7 show the breakthrough curves and cumulative sorption mass for As(III) and As(V) under different compressive pressures.

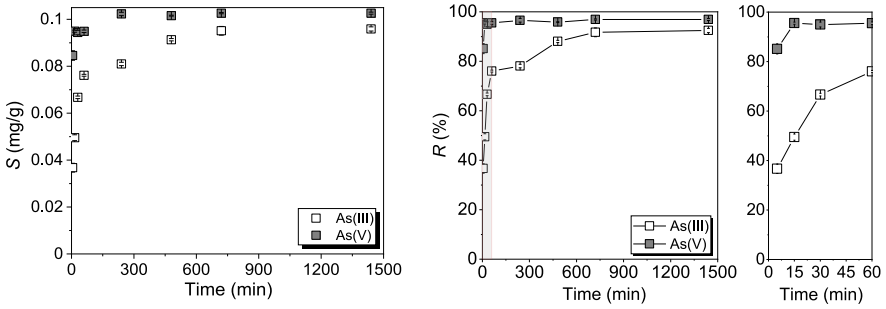

Fig. 3. Effect of contact time on the sorption performance of As (III) and As(V). (a) Sorption mass; (b) Removal percentage.

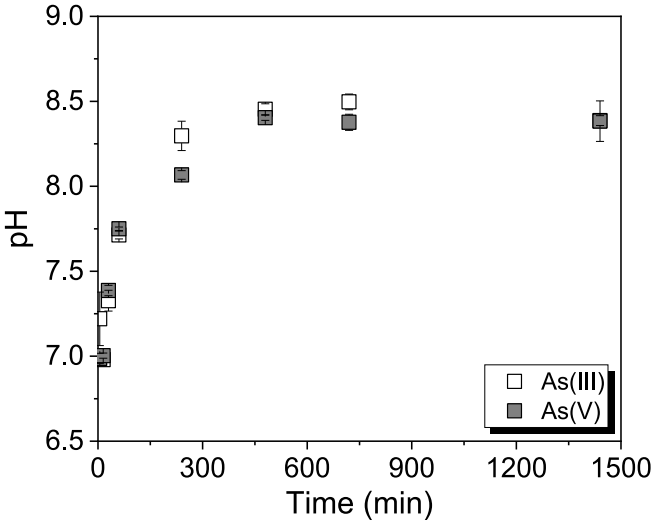

Fig. 4. PH value in solution during batch sorption tests.

Table 3 summarizes the effects of different compressive stresses obtained from breakthrough (Fig. 6) and cumulative sorption mass curves (Fig. 7). For As(III) cases, two loading levels of 10 and 200 kPa were used, while three different initial compressive stresses of 10, 100, and 200 kPa were used for As(V). The breakthrough curves were obtained by recording the effluent to influent concentration ratio (C/C_0 ratio) against the permeated influent volume. The breakthrough point is defined as the point when the effluent concentration reaches the regulatory limit of As in Japan (0.01 mg/L), that is thus $C/C_0 = 0.1$. The point where the C/C_0 ratio reaches 0.95 is called to be the exhaustion point, in which sorption saturation is considered to be achieved (Imbrogno and Schfer, 2021; Xing et al., 2011). For reference, two horizontal dotted lines representing the concentration of 0.1 C_0 and 0.95 C_0 were drawn in Fig. 6. In the whole sorption phase, as presented in Fig. 6(b), prior to the breakthrough, the effluent concentration was initially minimal, and then it increased over time until the breakthrough point. After the breakthrough point, the As concentration in the effluent increases gradually until the attainment of the exhaustion point and finally tends to be flat. The pH value of the effluent during the entire column experiments was also determined and the results are shown in Fig. 8. The data indicate that, during the sorption phase, the pH values in all cases decreased from a maximum at ~ pH 8 to a plateau fluctuating in the range of 6.5–7 (This pH change may be due to the dissolution of the hydrotalcite. See the explanation in Section 3.3.).

Fig. 7 shows the cumulative sorption mass under different compressive stress in both As(III) and As(V) cases. Specifically, as shown in Table 3, when $C/C_0 = 0.95$, the cumulative sorption mass of As(III) were 0.83 and 0.94 mg/g for 10 and 200 kPa cases, respectively, while those of As(V) increased from 22.0 to 24.3 mg/g. These obtained results suggested that the presence of compressive stress plays a slightly positive role in the sorption performance of this geosynthetic sorption sheet. This can also be proved by the results of the breakdown curves of As(V) sorption at different loading stresses in Fig. 6(b). As observed, the influent volumes at the breakthrough point ($C/C_0 = 0.1$) were found to be 9.5, 12.4, and 14.2 L for the loading stresses of 10, 100, and 200 kPa, respectively. As a result, more volume of water is treated before the breakthrough point as the increase of compressive stress.

Significantly, the breakthrough curves presented in Fig. 6 demonstrate a partial overlap between different compressive stresses,

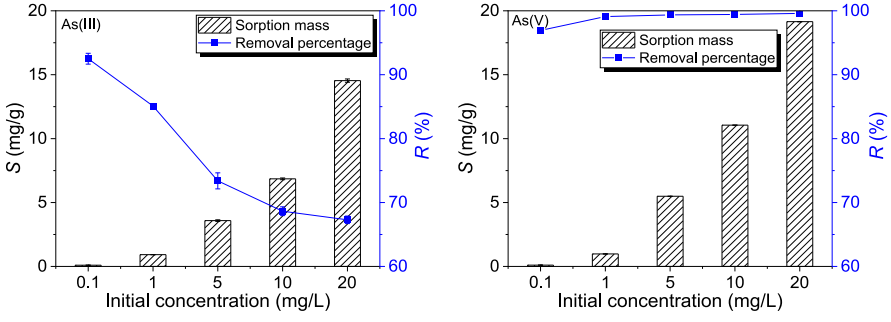

Fig. 5. Effect of initial concentration on sorption mass and removal percentage of As. (a) As(III); (b) As(V).

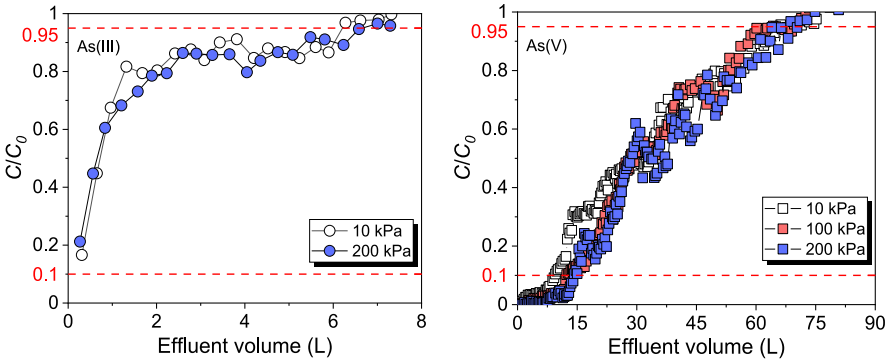

Fig. 6. Breakthrough curves subjected to different compressive stresses. (a) As(III); (b) As(V).

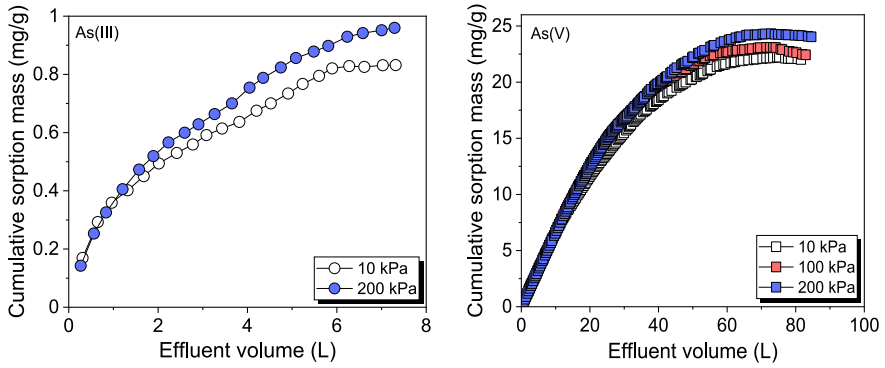

Fig. 7. Effect of compressive stress on the As cumulative sorption mass. (a) As(III); (b) As(V).

Table 3
Summary of cumulative sorption mass and permeated influent volume at breakthrough and exhaustion points for As(III) and As(V) sorbed onto the geosynthetic sorption sheet.

	Compressive stress (kPa)	$C/C_0 = 0.1$ (breakthrough point)		$C/C_0 = 0.95$ (exhaustion point)	
		Cumulative sorption mass (mg/g)	Effluent volume (L)	Cumulative sorption mass (mg/g)	Effluent volume (L)
As(III)	10	–	–	0.83	6.3
	200	–	–	0.94	6.6
As(V)	10	6.3	9.5	22.0	67.8
	100	8.2	12.4	23.1	69.6
	200	9.3	14.2	24.3	71.0

particularly in the As(III) cases, which seemingly contradicts the increasing trend of sorption mass observed in Fig. 7 for both As(III) and As(V). It should be emphasized that the breakthrough curves in Fig. 6 provide information on the effluent volume required to achieve a specific arsenic concentration in the effluent, while the cumulative sorption mass in Fig. 7 represents the total amount of arsenic sorbed by the geosynthetic sorption sheet throughout the entire test duration. As a result, the breakthrough curves for different compressive stresses may overlap, while the cumulative sorption mass still exhibits a clear trend of increase with increasing compressive stress. This overlapping could imply that the impact of compressive stress on the sorption performance of the geosynthetic sorption sheet was not substantial enough to produce a discernible difference in the effluent concentrations of arsenic (As(III) and As(V)) at the same effluent volume. Nonetheless, the results of cumulative sorption masses in Fig. 7 provide a more precise representation of the favorable influence of compressive stress on the sorption performance. Overall, these findings indicate that applying higher compressive stress can enhance the sorption performance of the geosynthetic sorption sheet, although to a limited extent, which has implications for arsenic removal applications. However, to fully understand the extent of the effect of compressive stress on the sorption performance of geosynthetic sorption sheets, further investigation through statistical analysis may be necessary to provide additional evidence to support these findings.

Fig. 9(a) and (b) illustrate SEM images of the distribution of fibers for geosynthetic sorption sheets under 0 and 200 kPa, respectively. The comparison of the two figures clearly indicates that the arrangement of fibers is changed before and after vertical loading. Before applying the loading, the fibers are distributed in a fairly sparse manner within the fabric layer of the geosynthetic sorption sheet. Only a few neighboring fibers are in direct contact with each other, with a high proportion of void space. While more compacted, bent and involved configurations of

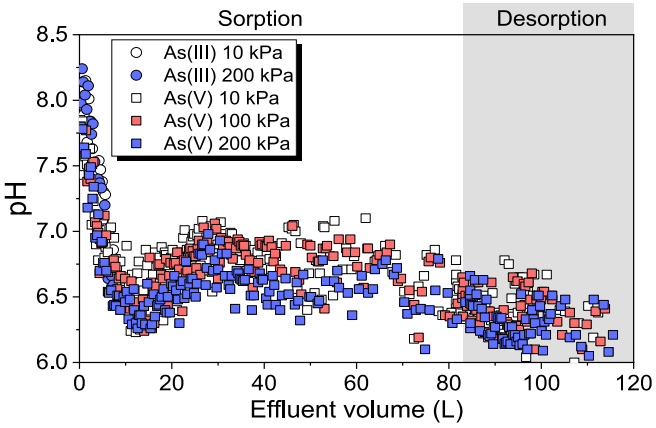

Fig. 8. The effluent pH during column tests.

fibers can be observed after the applied vertical loading, leading to a reduction in the number of large pores, as the higher entanglement of fibers covers the large pores with adjacent fibers. The high compression of the sheet leads to reduced average pore size and pore volume inside the fabric structure and is accompanied by the increasing growth in density, which forms a more effective contact between the arsenic solution and the sorbent in the sorption material layer.

In addition to the compression of the fiber web, intrusion of the upper fabric layer into the hydrotalcite layer is also responsible for the improvement in sorption performance. The hydrotalcite layer of the geosynthetic sorption sheet was also qualitatively characterized via SEM, as shown in Fig. 9(c). Microscopy showed that the hydrotalcite layer was an integration of sorbent materials with non-woven fabric scaffolds. Despite a uniform hydrotalcite-coat formed in the pore space being obtained, a small amount of μm-wide voids still exist in the coating. Fibers in the fabric layer were easily "squeezed" into the voids of the hydrotalcite layer upon the application of vertical stresses. This can be also seen in Fig. 9(d), which displays a close-up view of the hydrotalcite layer with a magnification of 350 times. The intrusion into the hydrotalcite layer occupied part of the void existing in the hydrotalcite-coat and thus increased the effective contact area. Because of this mechanism, the sorption performance could be improved with the increasing compressive stress.

Furthermore, the loading-induced magnitudes of the growth in cumulative sorption mass differ significantly at breakthrough and exhaustion points (Table 3). The geosynthetic samples subjected to higher stress levels gave larger values of cumulative sorption mass than the samples under lower stress levels, and the difference is less pronounced along with the experiment process. There was a trend such that the influence of compressive stress on the cumulative sorption mass obviously waned at the later stage of the experiment. For example, for As (V) cases subjected to 10, 100, and 200 kPa, a great extent of increment in cumulative sorption mass was observed at the breakthrough point (when $C/C_0 = 0.1$), around 47.6%; while when $C/C_0 = 0.95$ (at exhaustion points), the growth of cumulative sorption mass dropped to 10.5%. The results indicate that the impact of loading variations on the sorption performance of this material decreases significantly with the increase of influent volume. This is closely related to the changes in the porosity of the geosynthetic sorption sheet under compressive stress.

From the microscopic view (Fig. 9), the geosynthetic sorption sheet is a solid-pore complex composed of fibers and void space formed between fibers. For non-woven geotextiles, porosity is mainly used to investigate structural changes and hydraulic performance of geotextiles after compression, which is defined as the ratio of void volume to total volume. Variations in thickness and porosity of geosynthetic sorption sheets subjected to different vertical loadings are presented in Table 4. As may have been expected, the decline in thickness was larger for higher void space existing within fibers when a lower loading was used at the initial stage, and then the decline gradually became very small with the increased loading, resulting in reduced internal voids and higher bulk density (Ding et al., 2021b; Kothari and Das, 1994). In the later period, void space was sufficiently small, and the fiber structure itself was compressed, with no significant changes in the thickness.

The analytical comparison of As(III) and As(V) sorption onto the geosynthetic sorption sheet was also examined. In Fig. 7, cumulative sorption mass curves for loaded As(III) and As(V) cases revealed a uniform profile, reached a plateau at the cumulative flow volume of around 6 and 70 L, respectively, and then became essentially stable, which is in accord to the result presented in Fig. 6. As illustrated in Fig. 6, it can be seen that when As (III) cases reached the exhaustion point, all As (V) cases were far from the breakthrough point. For example, when the influent volume reached about 6 L, both loaded As (III) samples were at the exhaustion point ($C/C_0 = 0.95$), while the C/C_0 values of all As(V) samples under a compressive state were still relatively low, only 0.04 (10 kPa), 0.03 (100 kPa) and 0.01 (200 kPa) respectively. It is observed

Table 4
Variations in thickness and porosity of the geosynthetic sorption sheet under different loadings.

Compressive stress (kPa)	Thickness (mm)	Thickness change (mm)	Porosity (–)
0	2.8	–	0.79
10	2.3	0.5	0.73
100	1.6	1.2	0.62
200	1.2	1.6	0.49

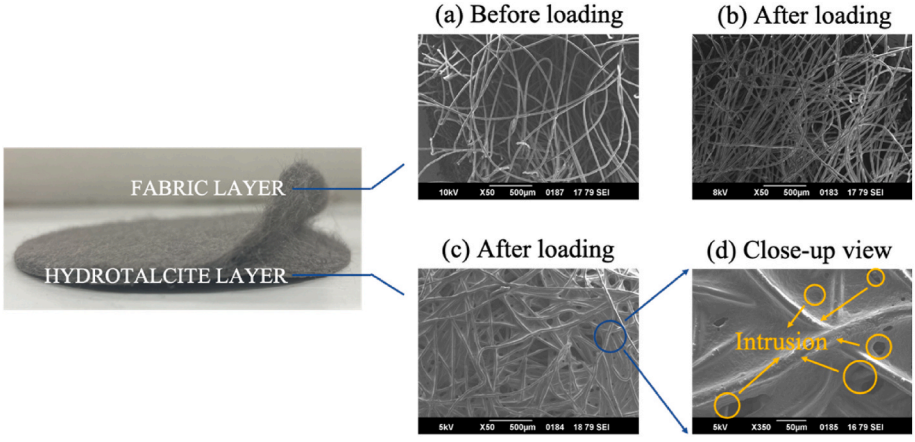

Fig. 9. The SEM image of the geosynthetic sorption sheet before and after loading.

that the geosynthetic sorption sheet shows a better sorption performance for As(V) compared with As(III). Through the comparison of cumulative sorption mass for As(III) and As(V) cases under different compressive stresses, as shown in Table 3, likewise, it can be seen that the cumulative sorption masses of As(V) cases are approximately 26.5 times (10 kPa) and 25.9 times (200 kPa) of As(III) cases respectively. Such results represent that the geosynthetic sheet is more suitable for As (V) sorption, verifying the results obtained from batch sorption experiments.

The differences in sorption behavior between As(III) and As(V) may be related to the different oxidation states of As (Yang et al., 2005). As (III) is primarily presented as H_3AsO_3, $H_2AsO_3^-$, $HAsO_3^{2-}$, and AsO_3^{3-} at the reducing conditions, and As(V) is dominant in the forms of H_3AsO_4, $H_2AsO_4^-$, $HAsO_4^{2-}$, and AsO_4^{3-} under oxidizing conditions (Yang et al., 2006; Grover et al., 2010). Arsenic speciation in aqueous solution largely depends upon the solution pH and the relationship between these two has been well documented (Dias et al., 2019; Mohan and Pittman, 2007; Smedley and Kinniburgh, 2002; Wang and Mulligan, 2006). The speciation of As(III) and As(V) in the solution is controlled by the chemical reactions and presented in Eqs. 6–10 for As(III) and Eqs. 11–14 for As(V) (Halter and Pfeifer, 2001):

$$NaAsO_2 = Na^+ + AsO_2^- \quad (6)$$

$$AsO_2^- + 2OH^- = AsO_3^{3-} + H_2O \quad (7)$$

$$AsO_2^- + OH^- = HAsO_3^{2-} \quad (8)$$

$$AsO_2^- + H_2O = H_2AsO_3^- \quad (9)$$

$$AsO_2^- + H_2O + H^+ = H_3AsO_3 \quad (10)$$

$$Na_2HAsO_4 = 2Na^+ + H^+ + AsO_4^{3-} \quad (11)$$

$$AsO_4^{3-} + H^+ = HAsO_4^{2-} \quad (12)$$

$$AsO_4^{3-} + 2H^+ = H_2AsO_4^- \quad (13)$$

$$AsO_4^{3-} + 3H^+ = H_3AsO_4 \quad (14)$$

where $NaAsO_2$ and Na_2HAsO_4 are used for preparing As(III) and As(V) solutions in this study, respectively, as described in Section 2.1. The pH value of the effluent during the column sorption phase decreased from approximately pH 8 to a range of 6.5–7, as illustrated by the monitoring results in Fig. 8. Most pentavalent arsenate species were reported to exist with negatively charged ionic forms ($HAsO_4^{2-}$ and $H_2AsO_4^-$) in the pH 6.5–8 range, whereas, for trivalent arsenite species, the neutral form H_3AsO_3 predominates. Since the interlayer anion exchange is a classical mechanism of hydrotalcite materials to achieve sorption, the negatively charged arsenate species are expected to be more easily sorbed by the hydrotalcite structure through anion exchange in comparison with the arsenites (Yang et al., 2005; Lazaridis et al., 2002). On the other hand, this may be due to the greater affinity of hydrotalcite for divalent anions, which are more prone to intercalate into hydrotalcite interlayers than monovalent anions, as explained in several previous studies (Constantino et al., 2018; Vágvolgyi et al., 2008).

The hydrotalcite in the geosynthetic sorption sheet used in this study is chloride hydrotalcite (as detailed in section 2.1), in which chloride ions exist as interlayer anions. Therefore, the primary mechanism for arsenic sorption on this geosynthetic material is the exchange of chloride ions in the interlayer, with the arsenic species incorporated into the interlamellar space (Nakamura et al., 2021; Bujdosó et al., 2009). Earlier research confirmed that chloride ions interlayered in hydrotalcite are exchanged with arsenic ions in the solution during the sorption process by evaluating the chloride ions concentration in the filtrate (Nakamura et al., 2021). For this study, the electric conductivity (EC) in the effluent solution was measured, which is closely related to the concentration of ions present in the solution. The monitored EC results are shown in Fig. 10. As observed, the EC in the effluent decreased with effluent volume and finally went plateaued. However, the measurement of chloride ions concentration in the effluent solution was not involved in the experiments in this study, which consequently meant that the EC values alone would not adequately support the release of interlayer anions from the hydrotalcite in the geosynthetic sorption sheet. Thus, the correlation between the release of chloride ions into the solution and the EC values in the solution is well worth exploring. Therefore, further research is required to confirm the liberation of the replaced interlayer anions in the effluent solution, which would provide a more comprehensive understanding of the sorption mechanism of the geosynthetic sorption sheet.

The oxidation-reduction potential (ORP) also plays a crucial role in controlling the aqueous speciation of arsenic, similar to the pH value (Smedley and Kinniburgh, 2002). The variation in relative proportions of As(III) and As(V) occurs when the geochemical environment becomes anaerobic (Peterson and Carpenter, 1983; Cai et al., 2022). Especially in employing geosynthetic sorption sheets in embankment constructions or temporary storage facilities, typically characterized by anoxic environments, the prevalence of As(III) may become increasingly significant owing to a sequence of reduction reactions, even though As(V) is generally the dominant species (Tabelin et al., 2012b). Tabelin et al. (2012b) reported that the pH of leachate generated from excavated altered rocks under anoxic conditions ranges from 7.5 to 9.5. In this pH range and under reducing conditions, the uncharged arsenic species (H_3AsO_3) is expected to be the predominant form of As(III) (Smedley and Kinniburgh, 2002). This indicated the limitations of the hydrotalcite-coated geosynthetic sorption sheet for As(III) removal in certain geochemical environments. Therefore, future research is needed to explore other effective treatment strategies for arsenic removal in different geochemical environments.

3.2.2. Desorption phase

In the desorption tests, distilled water was used as a desorbent and the effluent As(V) concentration was determined and shown in Fig. 11. The sorption and desorption curve for porous stones is presented in Fig. 11(a). The independent experiment for evaluating the sorption and desorption performance of porous stones indicates that the As(V) sorption capacity of porous stones can be negligible, and the existence of porous stones did not interfere with the sorption-desorption analysis for the geosynthetic sorption sheet. In the sorption stage, because porous

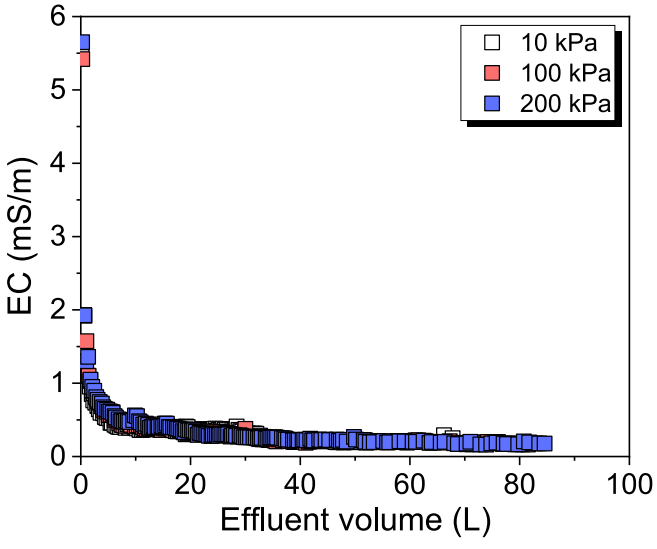

Fig. 10. EC value in effluent solution during column tests.

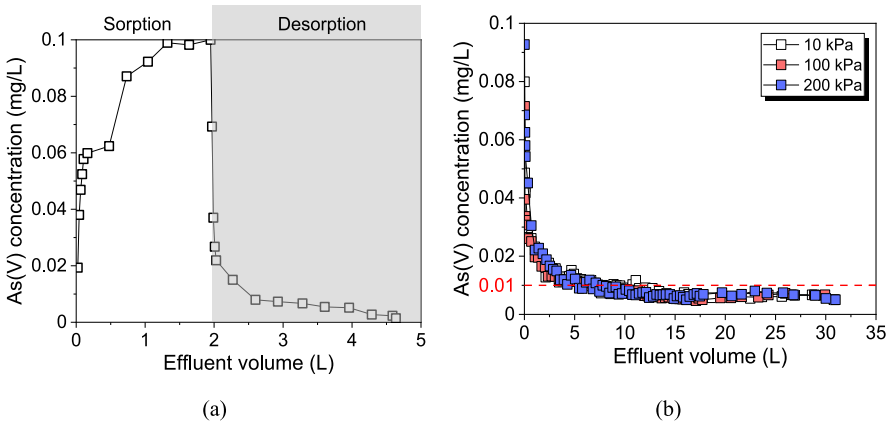

Fig. 11. Sorption and desorption results from porous stones and geosynthetic sorption sheets. (a) Porous stones; (b) geosynthetic sorption sheet.

stones had no sorption performance to As(V), As(V) rapidly passed through the porous stones. Hence, the effluent concentration was quickly equilibrated with the influent concentration. As the desorption effluent volume reached 4.6 L, the effluent concentration approached 0 and the desorption process was finished. This result also confirms that arsenic is not trapped and remains in porous stones used in this study.

Fig. 11(b) shows the desorption results of As(V) from the geosynthetic sorption sheet under various compressive stresses. During the desorption process, it can be observed that the desorption curves from three compressive stresses presented a very similar geometry, with a firstly rapid decrease in effluent concentration, followed by a gradually slender decrease, and became almost stable. When the effluent volume reached around 5–7 L, the effluent concentrations for all the cases were lower than 0.01 mg/L. The final desorption masses of As(V) under loading of 10, 100, and 200 kPa were approximately 0.81, 0.71, and 0.72 mg/g, respectively. The data suggests that the desorption mass is significantly lower than the sorption mass, which may be due to the exclusive sorption of As by hydrotalcite, resulting in irreversible sorption (Liang et al., 2022; Dias and Fontes, 2020). In addition, the desorption behavior should be associated with compressive stress. As shown in Fig. 12, the desorption ratio of As(V) decreased from 3.7% to 3.0% with increasing compressive stress. Similarly, comparing the calculated immobility of As(V) on the geosynthetic sorption sheet can reveal that the immobilized As(V) increased with increasing compressive stress, changing from 21.2 to 23.6 mg/g. As shown in Fig. 11(b), when $C = 0.01$ mg/L, the effluent volume obtained for different loading states (10, 100, and 200 kPa) were 7.3, 6.9, and 5.4 L, respectively, which led to the conclusion that the higher loading case realized its desorption equilibrium more rapidly than the lower one.

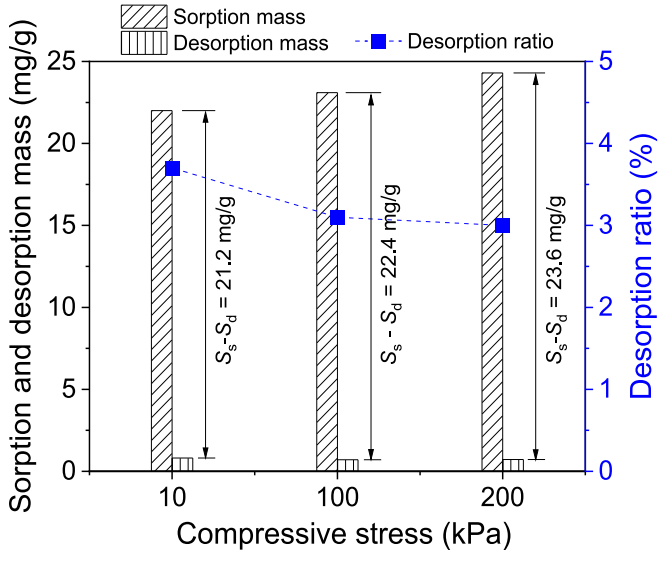

Fig. 12. Sorption and desorption mass and desorption ratio of As(V) from geosynthetic sorption sheet under different compressive stresses.

3.3. *Mineral stability of hydrotalcite contained in geosynthetic sorption sheets*

Mineral stability is generally an important concern in terms of the practical application of hydrotalcite-based material in the aqueous matrix (Goh et al., 2008; Dias and Fontes, 2020). To assess the stability of the hydrotalcite, the chemical properties of the effluent were monitored throughout the column tests. Fig. 8 shows the changes in effluent pH in column tests. As presented in Fig. 8, during the sorption phase, the pH values for all cases were ~pH 8 initially and then gradually decreased to ~pH 6.5; while in the desorption stage, the pH values slightly fluctuated around 6.5. This pH change may be attributed to hydrotalcite dissolution, as demonstrated by the existence of Mg and Al ions in the effluent illustrated in Fig. 13. As observed, the concentration of Mg in the effluent decreased with effluent volume and finally went below the detection limit of ICP-OES (0.1 mg/L); the Al concentration, on the other hand, could be detected only at a very early stage (effluent volume was less than 2 L) and after that only dissolution of Mg was observed. According to the quantitative analysis by Goh and Lim (2010), under the neutral condition, the release rate of Mg ranged between 0.1

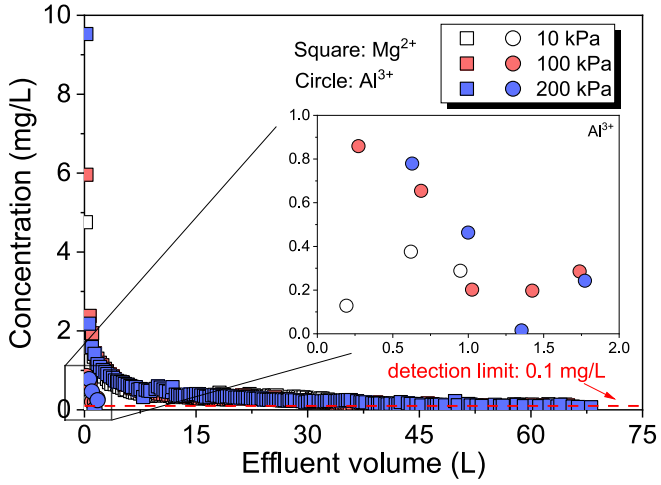

Fig. 13. Mg and Al concentration in the effluent during column tests.

and 1.3%, while that of Al was below 0.2%. This discrepancy in solubility is strongly affected by the properties of constituent cations (Allada et al., 2002). As a more soluble divalent ion, some researchers argued that the release of Mg and variation of its concentration might become a valuable indicator in evaluating the stability of the hydrotalcite (Jobbágy and Regazzoni, 2011). The significantly low release of Al from the hydrotalcite was probably caused by the formation of amorphous Al $(OH)_3$ (Allada et al., 2002). Thermodynamically, in the pH range of 5.0–9.0, the aqueous phase is supersaturated with respect to amorphous $Al(OH)_3$, and the expression for the dissolution is accounted for by (Maziarz et al., 2019):

$$\left[Mg^{2+}_{1-x}Al^{3+}_{x}(OH)_2\right]Cl^{-}_{x} + (2-3x)H^{+} \rightarrow (1-x)Mg^{2+} + xAl(OH)_3 + xCl^{-} + (2-3x)H_2O \quad (15)$$

Notably, as shown in Fig. 13, hydrotalcite showed a relatively evident dissolution of cationic components in the initial period of experiments (4.8–9.5 mg/L for Mg and 0.1–0.9 mg/L for Al within 0.3 L effluent volume), which may be partly ascribed to the dissolution of a tiny fraction of poorly crystallized hydrotalcite or Mg or Al precursor salts remaining in the hydrotalcite (Goh and Lim, 2010). Although some of the precursor metals have not been subjected to proper regulation, it would have to be guaranteed that their releases into the solution are lower than the harmful levels to the environment (Goh et al., 2008). Aluminum has aroused attention for its potential factor associated with the development of Alzheimer's disease (Dias and Fontes, 2020). In Japan, the latest Drinking Water Quality Standards (DWQS) prescribe a concentration limit of 0.2 mg/L for Al levels. In this study, Al releases from the hydrotalcite (Fig. 13) at the early stages of the dissolution are slightly above the standard value of the DWQS. In view of this, Yang et al. (2006) proposed a conditioning procedure named "adsorbent conditioning", which is specifically designed for the hydrotalcite with higher Mg and Al releases. This conditioning procedure is carried out before using hydrotalcite to reduce Mg and Al dissolution. Major operations include stirring the hydrotalcite in deionized water for 24 h (deionized water is changed every 6 h) and drying at room temperature for 12 h. However, it is also worth highlighting that hydrotalcite would gradually become stable with negligible releases of Mg and Al during continuous use (Goh et al., 2009). In particular, during the desorption process, the release of sorbed As(V) from the geosynthetic sorption sheet is significantly low (Fig. 11(b)), which gives this material an attractive property.

In fact, the stability of hydrotalcite-based materials is related to the surrounding conditions (Maziarz et al., 2019). Some research indicated that the dissolution of precursor metals could be induced in acidic conditions (Frost and Griffin, 1977; Terry, 2004; Ferreira et al., 2006; Goh et al., 2008). Despite the fact that hydrotalcite dissolution could be detrimental to the environment, few studies have been involved in the mineral stability of hydrotalcite in the sorption process (Dias and Fontes, 2020; Jobbágy and Regazzoni, 2011). This would therefore raise doubts about the use and applicability of such materials in a practical application context, especially in the absence of a deep analysis of their stability. For this study, pH adjusting was not involved in the experimental condition. The experimental results revealed that the hydrotalcite showed relative stability in neutral and slightly alkaline conditions. Thus, further research is required to confirm the stability of this material in a wider environmental background, which would be useful for evaluating the viability of the geosynthetic sorption sheet in practical application.

4. Conclusions

Adsorbent-containing geosynthetic sheets are the newly emerging areas of research, especially in attenuation layer methods. Considering its application in either embankment constructions or temporary storage facilities as an attenuation sorption layer, the overburden loading is a factor that should be considered. Therefore, the attenuation performance of the geosynthetic sorption sheet under different loadings has been experimentally investigated in the present study. A novel testing device was reformed for performing sorption-desorption column tests under mechanical loading. The main findings of this study can be drawn as follows.

(1) The presence of compressive stress plays a positive role in the sorption performance of this geosynthetic sorption sheet. More volume of water was treated before the breakthrough point and exhaustion point as the increase of compressive stress. This phenomenon can be attributed to the overall change within the fiber structure of the geosynthetic sorption sheet caused by vertical loading. More compacted, bent, and involved configurations of fibers can be observed after the applied vertical loading, leading to a reduction in the average pore size and pore volume inside of the fabric structure, which formed a more effective contact between the arsenic solution and the sorbent in the sorption material layer.

(2) As(III) is much more difficult to remove than As(V) by the geosynthetic sorption sheet. The cumulative sorption masses of As(V) cases are about 25.8–26.5 times greater than that of As(III) cases under all loading stresses, indicating that the geosynthetic sorption sheet shows a better sorption performance for As(V) compared with As(III). The adsorbent contained in this geosynthetic sheet is hydrotalcite, and its mechanism is interlayer anion exchange. The sorption discrepancy between As(III) and As (V) depends on the speciation distributions of As in the solutions. The negatively charged arsenate species ($HAsO_4^{2-}$ and $H_2AsO_4^{-}$) are expected to be more easily sorbed by the hydrotalcite structure through anion exchange in comparison with arsenites (neutral form H_3AsO_3 predominates).

(3) The desorption mass of As(V) was significantly lower than the sorption mass. The ultimate desorption ratios under three loading stresses are only 3.0–3.7%, indicating the As(V) is less prone to desorb from the geosynthetic sorption sheet. This can be interpreted by the exclusive sorption of As by hydrotalcite, resulting in irreversible sorption. Moreover, applied vertical loading also affects the desorption process. When $C = 0.01$ mg/L, the effluent volume obtained for different loading stresses (10, 100, and 200 kPa) were 7.3, 6.9, and 5.4 L, respectively. The obtained results reveal that the higher loading case realized its desorption equilibrium more rapidly than the lower one.

(4) The chemical analysis of effluent confirmed the presence of partial dissolution of hydrotalcite in the initial period of experiments, which led to increases in pH values. However, hydrotalcite would gradually become stable with negligible releases of cationic components during continuous use. On the other hand, the concentration ratio of the dissolved constituent cations (in our case, are Al^{3+} and Mg^{2+}) was not equal to that of the solid phase in the whole dissolution process, which is strongly affected by the properties of constituent cations.

The work done in this paper regarding the attenuation performance of geosynthetic sorption sheets is primarily concerned with the situation where the geosynthetic materials are applied under even loading. Indeed, in the application of geosynthetic sorption sheets to attenuation sorption layer methods, they are typically subjected to various types of complex, uneven loading conditions, which would lead to noticeable strain variations (Moo-Young and Tucker, 2002; Rowe and Yu, 2019; Tang et al., 2020; Feng et al., 2020). Pore sizes and permeability then may change over time during sustained strains and consequently influence the entire attenuation performance of geosynthetic sorption sheets (Fourie and Addis, 1999; Wu et al., 2008). Therefore, a thorough understanding of strain-induced variations in pore sizes and permeability is

of vital importance to predicting the attenuation performance of this geosynthetic material.

The interlayer anion exchange mechanism proposed for arsenic removal by hydrotalcite-coated geosynthetic sorption sheet, as discussed in Section 3.2.1, requires further research. Further research, such as analyzing the hydrotalcite microstructure before and after sorption tests and measuring chloride ion concentration in the effluent, could offer valuable insights into the interlayer anion exchange mechanism of hydrotalcite. However, the primary conclusion of this study, which demonstrates the effective sorption performance of geosynthetic sorption sheets for arsenic and the positive impact of compressive stress on arsenic sorption, remains valid and is supported by the available experimental data.

Furthermore, the hydrotalcite stability of the geosynthetic sorption sheet in an aqueous matrix has been addressed in Section 3.3, in which it is highly recommended to devote to additional studies on this field in a broader environmental context. So far, there are limited studies on the mineral stability of hydrotalcite in the sorption process. Further work will bridge this critical knowledge gap so as to take this geosynthetic material a step closer to field applications in the attenuation layer method.

Declaration of competing interest

The authors declare that they have no known competing financial interests or personal relationships that could have appeared to influence the work reported in this paper.

Data availability

Data will be made available on request.

Acknowledgment

The authors gratefully acknowledge the generous support provided by the JSPS KAKENHI (Grant numbers 22H00227 and 18H03797). The authors would also like to sincerely thank Mr. Tanaka S., Mr. Shimoda K., and Mr. Nakamura A. of Toyobo, Co., Ltd. For providing the geosynthetic sorption materials used in this study.

References

Allada, R.K., Navrotsky, A., Thompson-Berbeco, H., Casey, W.H., 2002. Thermochemistry and aqueous solubilities of hydrotalcite-like solids. Science 296 (5568), 721–723.
Basu, A., Saha, D., Saha, R., Ghosh, T., Saha, B., 2014. A review on sources, toxicity and remediation technologies for removing arsenic from drinking water. Res. Chem. Intermed. 45 (11), 447–485.
Buccino, M., Daliri, M., Calabrese, M., Somma, R., 2021. A numerical study of arsenic contamination at the Bagnoli bay seabed by a semi-anthropogenic source. Analysis of current regime. Sci. Total Environ. 782, 146811.
Bujdosó, T., Patzkó, A., Galbács, Z., Dékány, I., 2009. Structural characterization of arsenate ion exchanged MgAl-layered double hydroxide. Appl. Clay Sci. 44 (1–2), 75–82.
Cai, D., Kong, S., Shao, Y., Liu, J., Liu, R., Wei, X., Bai, B., Werner, D., Gao, X., Li, C., 2022. Mobilization of arsenic from As-containing rion minerals under irrigation: effects of exogenous substances, redox condition, and intermittent flow. J. Hazard Mater. 129736.
Constantino, L.V., Quirino, J.N., Abrão, T., Parreira, P.S., Urbano, A., Santos, M.J., 2018. Sorption–desorption of antimony species onto calcined hydrotalcite: surface structure and control of competitive anions. J. Hazard Mater. 344, 649–656.
Cui, J., Zhao, Y., Li, J., Beiyuan, J., 2018. Speciation, mobilization, and bioaccessibility of arsenic in geogenic soil profile from Hong Kong. Environ. Pollut. 232, 375–384.
Cutright, C., Finkelstein, R., Orlowski, E., Mclntosh, E., Brotherton, Z., Fabiani, T., Khan, S., Genzer, J., Menegatti, S., 2020. Nonwoven fiber mats with thermo-responsive permeability to inorganic and organic electrolytes. J. Membr. Sci. 616, 118439.
Dias, A.C., Fontes, M.F., Reis, C., Bellato, C.R., Fendorf, S., 2019. Simplex-Centroid mixture design applied to arsenic(V) removal from waters using synthetic minerals. J. Environ. Manag. 238, 92–101.
Dias, A.C., Fontes, M.P.F., 2020. Arsenic (V) removal from water using hydrotalcites as adsorbents: a critical review. Appl. Clay Sci. 191, 105615.
Ding, Z., Babar, A.A., Wang, C., Zhang, P., Ding, B., 2021. Spunbonded needle-punched non-woven geotextiles for filtration and drainage applications: manufacturing and structural design. Compos. Commun. 25, 100481.
Ding, Z., Wang, C., Babar, A.A., Liu, G., Ding, B., 2021. Tailoring high efficiency polypropylene based composite geotextiles for dewatering fly ash slurries. Compos. Commun. 26, 100794.
Duan, H., Wang, J., Huang, Q., 2015. Encouraging the environmentally sound management of C&D waste in China: an integrative review and research agenda. Renew. Sustain. Energy Rev. 43, 611–620.
Duan, H., Miller, T.R., Liu, G., Tam, V., 2019. Construction debris becomes growing concern of growing cities. Waste Manage. (Tucson, Ariz.) 83, 1–5.
El-Sayed, G.O., 2011. Removal of methylene blue and crystal violet from aqueous solutions by palm kernel fiber. Desalination 272 (1), 225–232.
Feng, S., Chen, J., Chen, H., Liu, X., Zhou, A., 2020. Analysis of sand-woven geotextile interface shear behavior using dem. Can. Geotech. J. 57 (3), 433–447.
Ferreira, O., Moraes, S.D., Duran, N., Cornejo, L., Alves, O., 2006. Evaluation of boron removal from water by hydrotalcite-like compounds. Chemosphere 62 (1), 80–88.
Fourie, A.B., Addis, P.C., 1999. Changes in filtration opening size of woven geotextiles subjected to tensile loads. Geotext. Geomembranes 17 (5), 331–340.
Frost, R.R., Griffin, R.A., 1977. Effect of pH on adsorption of arsenic and selenium from landfill leachate by clay minerals. Soil Sci. Soc. Am. J. 41 (1), 53–57.
Gillman, G.P., 2006. A simple technology for arsenic removal from drinking water using hydrotalcite. Sci. Total Environ. 366 (2–3), 926–931.
Goh, K.H., Lim, T.T., Dong, Z., 2008. Application of layered double hydroxides for removal of oxyanions: a review. Water Res. 42 (6–7), 1343–1368.
Goh, K.H., Lim, T.T., Dong, Z., 2009. Enhanced arsenic removal by hydrothermally treated nanocrystalline Mg/Al layered double hydroxide with nitrate intercalation. Environ. Sci. Technol. 43, 2537–2543.
Goh, K.H., Lim, T.T., 2010. Influences of co-existing species on the sorption of toxic oxyanions from aqueous solution by nanocrystalline Mg/Al layered double hydroxide. J. Hazard Mater. 180, 401–408.
Grover, K., Komarneni, S., Katsuki, H., 2010. Synthetic hydrotalcite-type and hydrocalumite-type layered double hydroxides for arsenate uptake. Appl. Clay Sci. 48 (4), 631–637.
Haas, M., Mongeard, L., Ulrici, L., D'Aloa, L., Benedikt, M., 2021. Applicability of excavated rock material: a european technical review implying opportunities for future tunnelling projects. J. Clean. Prod. 315, 128049.
Halter, W.E., Pfeifer, H.R., 2001. Arsenic(V) adsorption onto α-Al_2O_3 between 25 and 70°C. Appl. Geochem. 16 (7–8), 793–802.
Imbrogno, A., Schfer, A.I., 2021. Micropollutants breakthrough curve phenomena in nanofiltration: impact of operational parameters. Sep. Purif. Technol. 267, 118406.
Inatomi, S., Ishikawa, M., Shimoda, K., Nishioka, K., Miyawaki, K., 2019. Evaluation of adsorption characteristics by sheet adsorption materials. In: The 25th Symposium on Soil and Groundwater Contamination and Remediation (In Japanese).
Jha, P.K., Tripathi, P., 2021. Arsenic and fluoride contamination in groundwater: a review of global scenarios with special reference to India. Groundw. Sustain. Dev. 13, 100576.
Jobbágy, M., Regazzoni, A.E., 2011. Dissolution of nano-size Mg–Al–Cl hydrotalcite in aqueous media. Appl. Clay Sci. 51 (3), 366–369.
Junior, I.L.C., Machado, C.S., Pletsch, A.L., Torres, Y.R., 2022. Sorption and desorption behavior of residual antidepressants and caffeine in freshwater sediment and sewage sludge. Int. J. Sediment Res. 3, 346–354.
Kato, T., Gathuka, L.W., Okada, T., Takai, A., Katsumi, T., Imoto, Y., Morimoto, K., Nishikata, M., Yasutaka, T., 2021. Sorption-desorption column tests to evaluate the attenuation layer using soil amended with a stabilising agent. Soils Found. 61 (4), 1112–1122.
Kato, T., Takai, A., Iwata, Y., Gathuka, L.W., Katsumi, T., 2023. Evaluating temperature effects on leaching behavior of geogenic arsenic and boron from crushed excavated rocks using shaking and nonshaking batch tests. Soils Found. 63 (1), 101274.
Katsumi, T., 2015. Soil excavation and reclamation in civil engineering: environmental aspects. Soil Sci. Plant Nutr. 61, 22–29.
Kothari, V.K., Das, A., 1994. Effect of dynamic loading on compressional behaviour of spunbonded non-woven fabrics. Geotext. Geomembranes 13 (1), 55–64.
Lazaridis, N.K., Hourzemanoglou, A., Matis, K.A., 2002. Flotation of metal-loaded clay anion exchangers. Part II: the case of arsenates. Chemosphere 47 (3), 319–324.
Liu, M., Zhang, X., Li, Z., Qu, L., Han, R., 2020. Fabrication of zirconium (IV)-loaded chitosan/Fe_3O_4/graphene oxide for efficient removal of alizarin red from aqueous solution. Carbohydr. Polym. 248, 116792.
Li, J., Kosugi, T., Riya, S., Hashimoto, Y., Hou, H., Terada, A., Hosomi, M., 2017. Use of batch leaching tests to quantify arsenic release from excavated urban soils with relatively low levels of arsenic. J. Soils Sediments 17, 2136–2143.
Li, J., Kosugi, T., Riya, S., Hashimoto, Y., Hou, H., Terada, A., Hosomi, M., 2018. Pollution potential leaching index as a tool to assess water leaching risk of arsenic in excavated urban soils. Ecotoxicol. Environ. Saf. 147, 72–79.
Liang, X., Liu, L., Jiang, Y., Nan, Z., Deng, X., Ma, F., Wang, G., Wu, Y., 2022. Study of the sorption/desorption behavior of chlortetracycline on sediments in the upper reaches of the Yellow River. Chem. Eng. J. 428, 131958.
Lieb, R.H., 2009. Materials management at the gotthard base tunnel-experience from 15 years of construction. Geomech. Tunn. 2 (5), 619–626.
Lima, J.Z., Silva, E.F., Patinha, C., Duraes, N., Vieira, E.M., Rodrigues, V.G.S., 2021. Sorption of arsenic by composts and biochars derived from the organic fraction of municipal solid wastes: kinetic, isotherm and oral bioaccessibility study. Environ. Res. 204, 111988 (Part A).
Lin, C., Zhang, X., Galinmoghadam, J., Guo, Y.P., 2022. Working mechanism of a new wicking geotextile in roadway applications: a numerical study. Geotext. Geomembranes 50 (2), 323–336.

Luo, J., Meng, X., Crittenden, J., Qu, J., Hu, C., Liu, H., Peng, P., 2018. Arsenic adsorption on α-MnO_2 nanofibers and the significance of (100) facet as compared with (110). Chem. Eng. J. 331, 492–500.
Maamoun, I., Eljamal, R., Falyouna, O., Bensaida, K., Sugihara, Y., Eljamal, O., 2021. Insights into kinetics, isotherms and thermodynamics of phosphorus sorption onto nanoscale zero-valent iron. J. Mol. Liq. 328, 115402.
Magnusson, S., Lundberg, K., Swedberg, B., Knutsson, S., 2015. Sustainable management of excavated soil and rock in urban areas: a literature review. J. Clean. Prod. 93, 18–25.
Maziarz, P., Matusik, J., Straczek, T., Kapusta, C., Woch, W.M., Tokarz, W., Radziszewska, A., Leiviska, T., 2019. Highly effective magnet-responsive LDH-Fe oxide composite adsorbents for As(V) removal. Chem. Eng. J. 362, 207–216.
Ministry of the Environment. Soil contamination Countermeasures: guidelines for the treatment of contaminated soil. Revised 4.1th Edition). http://www.env.go.jp/water//dojo/dojogl2021_3.pdf (in Japanese).
Mo, J., Flores, G., Inui, T., Katsumi, T., 2020. Hydraulic and sorption performances of soil amended with calcium-magnesium composite powder against natural arsenic contamination. Soils Found. 60 (5), 1084–1096.
Mohan, D., Pittman, C.U., 2007. Arsenic removal from water/wastewater using adsorbents–a critical review. J. Hazard Mater. 142 (1–2), 1–53.
Moosavi, S., Lai, C.W., Zamiri, G., Pivehzhani, O.A., Johan, M.R., 2020. Application of efficient magnetic particles and activated carbon for dye removal from wastewater. ACS Omega 5 (33), 20684–20697.
Moo-Young, H.K., Tucker, W.R., 2002. Evaluation of vacuum filtration testing for geotextile tubes. Geotext. Geomembranes 20 (3), 191–212.
Nakamura, T., Fujiwara, T., Ogata, F., Kawasaki, N., 2021. Synthesis of novel Mg–Al–Fe-type hydrotalcite with various Mg/Al/Fe ratios and its selective adsorption of As(V) from water. J. Environ. Chem. Eng. 9 (1), 104557.
Osono, A., Katoh, M., 2021. Characteristics of the immobilization process of arsenic depending on the size fraction released from excavated rock/sediment after the addition of immobilization materials. J. Environ. Manag. 298, 113534.
Peterson, M.L., Carpenter, R., 1983. Biogeochemical processes affecting total arsenic and arsenic species distributions in an intermittently anoxic fjord. Mar. Chem. 12 (4), 295–321.
Qian, J., Hu, Y., Zhang, J., Xiao, W., Ling, J., 2019. Evaluation the performance of controlled low strength material made of excess excavated soil. J. Clean. Prod. 214, 79–88.
Riviera, P.P., Bellopede, R., Marini, P., 2014. Bassani M. Performance-based re-use of tunnel muck as granular material for subgrade and sub-base formation in road construction. Tunn. Undergr. Space Technol. 40, 160–173.
Rowe, R.K., Yu, Y., 2019. Magnitude and significance of tensile strains in geomembrane landfill liners. Geotext. Geomembranes 47 (3), 439–458.
Sahu, S.J., Nath, B., Roy, S., 2011. A laboratory batch study on arsenic sorption and desorption on guava orchard soils of Baruipur, West Bengal, India. J. Geochem. Explor. 108 (2), 157–162.
Shimoda, K., Ishikawa, M., Nishioka, K., Kentaro, M., 2019. Countermeasure for heavy metal contaminated soil by natural origin. Geotech Eng Mag 67, 34–35 (In Japanese).
Smedley, P.L., Kinniburgh, D.G., 2002. A review of the source, behaviour and distribution of arsenic in natural waters. Appl. Geochem. 17 (5), 517–568.
Somma, R., Ebrahimi, P., Troise, C., Natale, G.D., Albanese, S., 2021. The first application of compositional data analysis (coda) in a multivariate perspective for detection of pollution source in sea sediments: the pozzuoli bay (Italy) case study. Chemosphere 274, 129955.
Tabelin, C.B., Igarashi, T., Tamoto, S., Takahashi, R., 2012. The roles of pyrite and calcite in the mobilization of arsenic and lead from hydrothermally altered rocks excavated in Hokkaido, Japan. J. Geochem. Explor. s 119–120, 17–31.
Tabelin, C.B., Igarashi, T., Yoneda, T., 2012. Mobilization and speciation of arsenic from hydrothermally altered rock containing calcite and pyrite under anoxic conditions. Appl. Geochem. 27 (12), 2300–2314.
Tabelin, C.B., Igarashi, T., Yoneda, T., Tamamura, S., 2013. Utilization of natural and artificial adsorbents in the mitigation of arsenic leached from hydrothermally altered rock. Eng. Geol. 156, 58–67.
Tabelin, C.B., Hashimoto, A., Igarashi, T., Yoneda, T., 2014. Leaching of boron, arsenic and selenium from sedimentary rocks: II. pH dependence, speciation and mechanisms of release. Sci. Total Environ. 473–474, 244–253.
Tabelin, C.B., Igarashi, T., Arima, T., Sato, D., Tatsuhara, T., Tamoto, S., 2014. Characterization and evaluation of arsenic and boron adsorption onto natural geologic materials, and their application in the disposal of excavated altered rock. Geoderma 213, 163–172.
Tabelin, C.B., Sasaki, R., Igarashi, T., Park, I., Tamoto, S., Arima, T., Ito, M., Hiroyoshi, N., 2017. Simultaneous leaching of arsenite, arsenate, selenite and selenate, and their migration in tunnel-excavated sedimentary rocks: I. column experiments under intermittent and unsaturated flow. Chemosphere 186, 444–454.
Tabelin, C.B., Igarashi, T., Villacorte-Tabelin, M., Park, I., Opiso, E.M., Ito, M., Hiroyoshi, N., 2018. Arsenic, selenium, boron, lead, cadmium, copper, and zinc in naturally contaminated rocks: a review of their sources, modes of enrichment, mechanisms of release, and mitigation strategies. Sci. Total Environ. 645, 1522–1553.
Tang, L., Tang, X.W., Liu, Y., Qu, S.X., 2020. Prediction of pore size characteristics of woven slit-film geotextiles subjected to unequal biaxial tensile strains. Geotext. Geomembranes 48 (5), 724–734.
Tangviroon, P., Hayashi, R., Igarashi, T., 2017. Effects of additional layer(s) on the mobility of arsenic from hydrothermally altered rock in laboratory column experiments. Water Air Soil Pollut. 228, 191.
Tatsuhara, T., Arima, T., Igarashi, T., Tabelin, C.B., 2012. Combined neutralization–adsorption system for the disposal of hydrothermally altered excavated rock producing acidic leachate with hazardous elements. Eng. Geol. 139–140, 76–84.
Technical Committee of Environmental Conservation Technology Association, Hokkaido 2012: Manual for Designing Sorption Layer Method, Technical Report of Hokkaido Environmental Conservation Technology Association No.5, in Japanese.
Terry, P.A., 2004. Characterization of Cr ion exchange with hydrotalcite. Chemosphere 57 (7), 541–546.
Vágvolgyi, V., Palmer, S.J., Kristóf, J., Frost, R.L., Horváth, H., 2008. Mechanism for hydrotalcite decomposition: a controlled rate thermal analysis study. J. Colloid Interface Sci. 318 (2), 302–308.
Wang, J.Y., Touran, A., Christoforou, C., Fadlalla, H., 2004. A systems analysis tool for construction and demolition wastes management. Waste Manage. (Tucson, Ariz.) 24 (10), 989–997.
Wang, S., Mulligan, C.N., 2006. Occurrence of arsenic contamination in Canada: sources, behavior and distribution. Sci. Total Environ. 366 (2/3), 701–721.
Wei, Y.T., Zheng, Y.M., Chen, J.P., 2011. Enhanced adsorption of arsenate onto a natural polymer-based sorbent by surface atom transfer radical polymerization. J. Colloid Interface Sci. 356 (1), 234–239.
Wu, C.S., Hong, Y.S., Wang, R.H., 2008. The influence of uniaxial tensile strain on the pore size and filtration characteristics of geotextiles. Geotext. Geomembranes 26 (3), 250–262.
Xing, X., Gao, B.Y., Zhong, Q.Q., 2011. Sorption of nitrate onto amine-crosslinked wheat straw: characteristics, column sorption and desorption properties. J. Hazard Mater. 186 (1), 206–211.
Yang, L., Shahrivari, Z., Liu, P.K.T., 2005. Removal of trace levels of arsenic and selenium from aqueous solutions by calcined and uncalcined layered double hydroxides (LDH). Ind. Eng. Chem. Res. 44 (17), 6804–6815.
Yang, L., Dadwhal, M., Shahrivari, Z., 2006. Adsorption of arsenic on layered double hydroxides: effect of the particle size. Ind. Eng. Chem. Res. 45 (13), 4742–4751.
Zhang, N., Duan, H., Sun, P., Li, J., Zuo, J., Mao, R., Liu, G., Niu, Y., 2020. Characterizing the generation and environmental impacts of subway-related excavated soil and rock in China. J. Clean. Prod. 248, 119242.
Zubair, M., Daud, M., Mckay, G., Shehzad, F., Al-Harthi, M.A., 2017. Recent progress in layered double hydroxides (LDH)-containing hybrids as adsorbents for water remediation. Appl. Clay Sci. 143, 279–292.
MLIT. Ministry of Land, Infrastructure, Transportation and Tourism: Results of the Survey on Construction Byproduct in Past Fiscal Years. available at: https://www.mlit.go.jp/sogoseisaku/region/recycle/d02status/d0201/page_020101census.htm. last access: 25 February 2022.